ChemComm

COMMUNICATION

View Article Online
View Journal | View Issue



Cite this: *Chem. Commun.*, 2019, **55**, 8832

Received 11th April 2019,
Accepted 24th May 2019

DOI: 10.1039/c9cc02819f

rsc.li/chemcomm



# Tuning of the flexibility in metal–organic frameworks based on pendant arm macrocycles†

Sungeun Jeoung,[a] Songho Lee,[a] Jae Hwa Lee,[a] Soochan Lee,[b] Wonyoung Choe,[b] Dohyun Moon *[c] and Hoi Ri Moon *[a]

**An isostructural series of flexible metal–organic frameworks based on macrocycles having diverse pendant arms was developed to tune flexibility depending on functional groups. The pendant arms directing into the pores were found to play a key role in imparting different gate-opening behaviours in the threshold pressure and sorption capacity upon interaction with guest molecules.**

The design and syntheses of metal–organic frameworks (MOFs) begin with the selection of the metal nodes and bridging organic ligands.[1] Types of metal and organic building blocks and the nature of their assembly determine the geometry and structure of the MOFs. Often, they allow a high degree of flexibility, resulting in so-called 'flexible MOFs' or 'soft porous crystals'.[2] Flexible MOFs can reversibly change their form upon the action of external stimuli, owing to the intermolecular degrees of freedom in their components and thus, have tremendous potentials in applications such as adsorption, separation, sensing, catalysis, and biomedical usage.[3] Accordingly, researchers studying MOFs have been devoting considerable efforts to establish the fundamental principles that facilitate the syntheses of flexible MOFs. For instance, the O–O axis of a carboxylate group endows significant breathing effect in MIL-53 and MIL-88 by acting as a kneecap.[4] Farha *et al.* recently reported a flexible MOF, NU-1400, based on four connected $Zr_6$ nodes, which afforded degrees of freedom by reducing the connectivity, compared with rigid NU-1000 and NU-901 having eight connected $Zr_6$ nodes.[5]

However, strategies for the incorporation of selective switching in flexible MOFs, as demanded by the applications based on the flexibility, are still elusive and serendipitous. Hence, designing and controlling the flexibility in these materials are essential and yet, a challenging issue. Several strategies have been demonstrated in order to tune the structural dynamics and responsiveness of the MOFs such as crystal size adjustment, metal substitution, and linker functionalization with various functional groups or flexible side chains.[6]

Macrocycle-based MOFs have been reported as a subclass of MOFs; in particular, aza-macrocyclic complexes with square planar geometry can act as a linear linker, providing axial sites for carboxylate ligands.[7] Furthermore, various types of functional groups can be easily introduced into the pores during the synthesis, by using macrocyclic moieties such as the 1,3,6,8,10,13-hexaazacyclotetradecane Ni(II) complex with pendant arms at 1 and 8 positions.[8] Previously, we reported a flexible MOF based on the Ni(II) macrocycle having two propyl arms that behaved as a molecular gate.[9] Experimental and theoretical studies found that $CO_2$ molecules mainly interacted with the propyl pendant arms to induce the gate-opening and breathing phenomena. Based on this, we postulated that such a MOF can be an excellent platform for easily securing different functional groups in the pendant arm macrocycles, which would render them different structural dynamics. Thus, we introduced nitrile, hydroxyl, and allyl pendant arms in Ni(II) macrocycles in this study and successfully synthesised three isostructural flexible MOFs, ***flex*-MOF(CN)**, ***flex*MOF(OH)**, and ***flex*MOF($CH_2$)** (Fig. 1). Upon types of the guest molecules such as $CO_2$ and water, these MOFs showed distinguishable flexible behaviours, which were examined by sorption isotherms, *in situ* X-ray powder diffraction (XRPD), and single-crystal diffraction (SCD).

To synthesise an isostructural series of flexible MOFs decorated with different functional groups, we induced the self-assembly of a tetradentate ligand, 2,2′,5,5′-biphenyltetracarboxylic acid ($H_4$BPTC), with $[NiL_R]^{2+}$ as a metal building block (R = CN, OH, and $CH_2$ for nitrile, hydroxyl, and allyl substitutes, respectively, Fig. 1a), yielding $\{[(NiL_{CN})_2(BPTC)]\cdot 4DMF\cdot 2H_2O\}$ (***as-flex*MOF(CN)**;

[a] *Department of Chemistry, Ulsan National Institute of Science and Technology (UNIST), 50 UNIST-gil, Ulsan 44919, Republic of Korea. E-mail: hoirimoon@unist.ac.kr*
[b] *Department of Chemistry, Ulsan National Institute of Science and Technology (UNIST), 50 UNIST-gil, Ulsan 44919, Republic of Korea. E-mail: choe@unist.ac.kr*
[c] *Beamline Division, Pohang Accelerator Laboratory, 80 Jigok-ro, 127beon-gil, Nam-gu, Pohang, Gyeongbuk 37673, Republic of Korea. E-mail: dmoon@postech.ac.kr*

† Electronic supplementary information (ESI) available: Experimental procedures, crystal structures, details of characterisation results. CCDC 1898504–1898507, 1908259 and 1908261. For ESI and crystallographic data in CIF or other electronic format see DOI: 10.1039/c9cc02819f

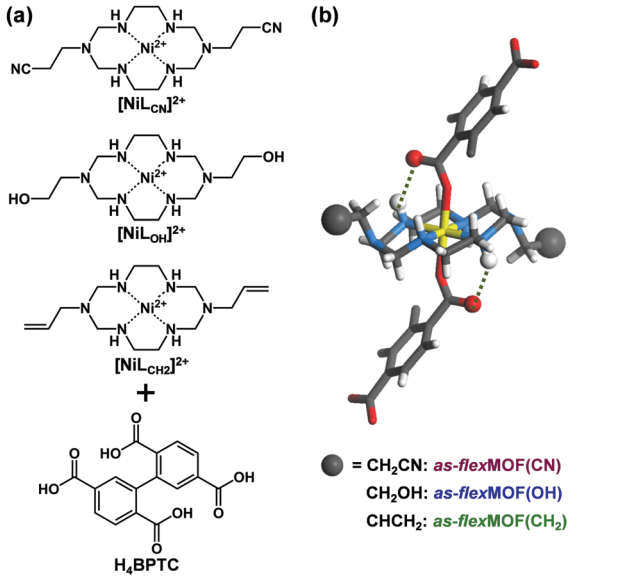


Fig. 1 (a) Square planar Ni(II) macrocycles with different pendant arms as metal building blocks and $H_4$BPTC as an organic building block. (b) Representation of the linear connectivity between two building units *via* coordinate and hydrogen bonds. Colour scheme: Ni, yellow; C, grey; O, red; N, blue; H, white.

DMF = *N*,*N*-dimethylformamide), $\{[(NiL_{OH})_2(BPTC)]\cdot 1DMF\cdot 3H_2O\}$ (***as-flex*MOF(OH)**), and $\{[(NiL_{CH2})_2(BPTC)]\cdot 1CH_3CN\cdot 5H_2O\}$ (***as-flex*MOF(CH$_2$)**). For all the compounds, the square planar Ni(II) macrocycles were coordinated by two $BPTC^{4-}$ ligands in the axial sites, resulting in a six-coordinated octahedral geometry with hydrogen bonds between the uncoordinated oxygen atoms of the carboxylate and secondary amines from the aza-macrocyclic complex (dotted lines in Fig. 1b). Since the $BPTC^{4-}$ moiety in the MOFs is not planar (dihedral angles between two phenyl rings are 52.780° in ***as-flex*MOF(CN)**, 50.318° in ***as-flex*MOF(OH)**, and 57.267° in ***as-flex*MOF(CH$_2$)**) and coordinates four macrocycles, 3D networks having interconnected pores are formed (top of Fig. S4–S6, ESI†), in which the void space is 52.5% for ***as-flex*MOF(CN)**, 49.6% for ***as-flex*MOF(OH)**, and 41.2% for ***as-flex*MOF(CH$_2$)** per unit cell volume, as obtained by *PLATON* calculations.[10] Upon drying the MOFs, the 3D structures drastically changed and exhibited structural flexibility, as evidenced by the XRPD patterns (Fig. S7–S9, and details of activation are provided in ESI;† hereafter, dried compounds are designated as ***cp-flex*MOF** (***cp*** = closed-pore)). The void volume is also greatly reduced to 6.1%, 6.6%, and 3.9% per unit cell volume for ***cp-flex*MOF(CN)**, ***cp-flex*MOF(OH)**, and ***cp-flex*MOF(CH$_2$)**, respectively. Despite such tremendous changes in the cell volume, all the samples maintained single crystallinity, which was sufficient to obtain SCD data. Fig. 2 shows that the rectangular dimension of ***as*** phases in all the three compounds considerably shrank in ***cp*** phases (42.6%, 34.1%, and 23.8% decreases for ***flex*MOF(CN)**, ***flex*MOF(OH)**, and ***flex*MOF(CH$_2$)**, respectively). During the dynamic movement, the dihedral angle between the two phenyl rings and those between the carboxylate planes and benzene rings of the ligand changed, and the pendant arms of the macrocycles blocked the pores (Fig. S10–S12, ESI†).

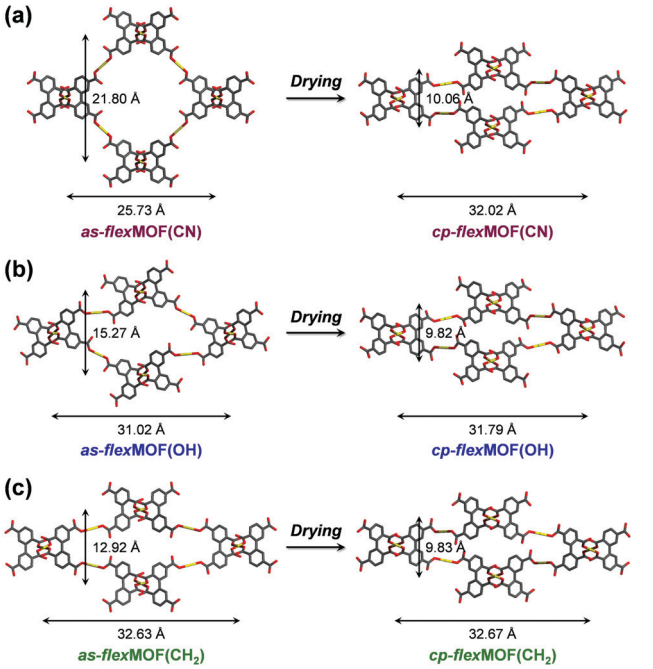


Fig. 2 Comparison between the as-synthesised (***as***) and closed-pore (***cp***) phases of (a) ***flex*MOF(CN)**, (b) ***flex*MOF(OH)**, and (c) ***flex*MOF(CH$_2$)** in rectangular dimension. The macrocycles and hydrogen atoms are omitted for clarity. Colour scheme: Ni, yellow; C, grey; O, red.

In order to explore the guest-dependent flexibility of these MOFs, $N_2$ and $CO_2$ gas sorption isotherms were obtained at 77 and 196 K, respectively. All ***cp*** phases showed typical type II $N_2$ sorption isotherms, indicating a nonporous nature (Fig. S13, ESI†). However, the characteristic of the $CO_2$ sorption isotherms was interesting (Fig. 3). ***cp-flex*MOF(CN)** exhibited gate-opening for $CO_2$ with an abrupt uptake at a threshold pressure of 0.42 bar, and its total adsorption capacity approached 40.1 wt% (204.8 cc g$^{-1}$ or 9.14 mmol g$^{-1}$ of the host) at 1 bar. When the allyl pendant arms are introduced, the resulting MOF, ***cp-flex*MOF(CH$_2$)** displayed a significantly different threshold pressure of ~0.70 bar, which was higher than that in ***cp-flex*MOF(CN)**. This was also accompanied by a decrease in the $CO_2$ uptake capacity (16.7 wt%, 85.5 cc g$^{-1}$, or 3.82 mmol g$^{-1}$). The different response of

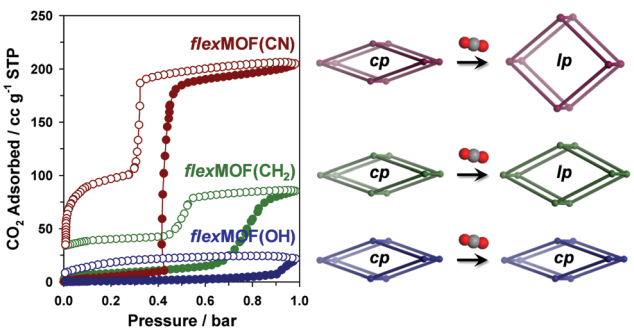


Fig. 3 $CO_2$ adsorption/desorption isotherms of ***flex*MOF(CN)**, ***flex*MOF(OH)**, and ***flex*MOF(CH$_2$)** at 196 K (left) and schematic of their flexible behaviours upon $CO_2$ adsorption (right). Filled and empty circles represent adsorption and desorption curves, respectively.

***cp-flex*MOF(CN)** and ***cp-flex*MOF($CH_2$)** toward $N_2$ and $CO_2$ can be explained by the high quadruple moment and polarizability of $CO_2$, which is in contrast to the inert nature of $N_2$.[11] It is also noteworthy that ***as*** phases of ***flex*MOF(CN)** and ***flex*MOF($CH_2$)** were estimated to potentially adsorb *ca.* 13.9 and 5.4 mmol $g^{-1}$ of $CO_2$, respectively (greater than the experimental value; Table S11, ESI†), as calculated by grand canonical Monte Carlo (GCMC) adsorption simulation performed with the molecular software package, RASPA 2.0 (details of simulation in ESI†).[12] This implies that those ***cp*** phases are not fully transformed into ***as*** phases under this condition (1 bar of $CO_2$ at 196 K), but are open up to form new phases, ***lp-flex*MOF** (Fig. 3; ***lp*** stands for large pore phase). Also, both the ***flex*MOF(CN)** and ***flex*-MOF($CH_2$)** desorbed in a hysteretic and stepwise manner, which adsorption and desorption curves do not merge at the end even under vacuum ($<10^{-5}$ mbar) at 196 K. In contrast, hydroxyl group-containing ***cp-flex*MOF(OH)** showed no stepwise adsorption profile with negligible uptake.

The forementioned different responsive behaviours were studied by *in situ* XRPD under the synchronized condition of $CO_2$ sorption. The XRPD patterns of ***cp-flex*MOF(CN)** did not change up to 0.4 bar, and a drastic structural change was observed at 0.6 bar, at which the $CO_2$ uptake increased sharply (Fig. S14, ESI†), retaining up to 1 bar. As mentioned previously, this is not a same structure with a ***as*** phase, but a ***lp*** phase. During desorption, the XRPD patterns were retained up to 0.4 bar, but it changed into a new structure below this pressure, which had neither ***cp*** nor ***lp*** structure and thereby denoted as ***np-flex*MOF(CN)** (Fig. 4a; ***np*** stands for narrow pore phase). Such a discovery of a new intermediate phase derived upon desorption has been very rarely reported in flexible MOFs.[13]

The intermediate structure, ***np-flex*MOF(CN)** has its own permanent porosity. After one adsorption–desorption experiment, the ***np*** phase is stabilised even under vacuum at 196 K. Interestingly, the successive measurement of the $CO_2$ uptake beginning from ***np-flex*MOF(CN)** at 196 K (Fig. 4b) showed type IV adsorption isotherm, which was clearly different from the adsorption isotherm of the first cycle. In this profile, even at the low pressure region $CO_2$ uptake was occurred up to 12.0 wt%, yet the threshold pressure was observed at the same position of the first cycle. The total $CO_2$ uptake decreased from 40.1 to 33.7 wt%, in which the uptake difference is equal to the trapped amount of $CO_2$ after the first cycle, and the desorption curve retraced to the adsorption curve. As revealed by the *in situ* XRPD (Fig. 4c), the ***np*** transformed to the ***lp*** phase during the $CO_2$ re-adsorption, and then reverted to its ***np*** phase after re-desorption. The further consecutive cycle of $CO_2$ adsorption/desorption for ***np-flex*MOF(CN)** fully reproduced this trend (Fig. S15, ESI†), indicating the reversible transition between the ***np*** and ***lp*** phases (Fig. 4a). Furthermore, heating at 110 °C under vacuum resulted in the transformation into the ***cp*** phase (Fig. 4c and Fig. S16, ESI†). Remarkably, at higher temperature (298 K), the ***np*** phase can be still identified upon $CO_2$ desorption (Fig. S19, ESI†). The gate-opening pressure of ***flex*MOF(CN)** dramatically shifts to a higher pressure upon the temperature increase to room temperature, while ***flex*MOF($CH_2$)** still opens the pores at a very low pressure.

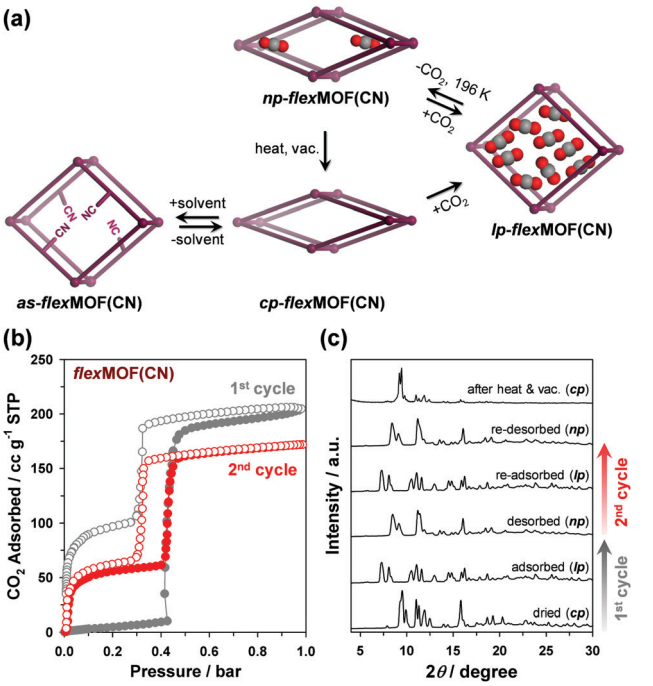


Fig. 4 (a) Schematic illustration of the phase transitions of ***flex*MOF(CN)** upon guest removal/reintroduction and $CO_2$ adsorption/desorption. (b) Consecutive cycles of $CO_2$ adsorption/desorption isotherms in ***flex*MOF(CN)** at 196 K, and (c) corresponding XRPD data measured before $CO_2$ adsorption, after adsorption, desorption (vacuum $< 10^{-5}$ mbar), re-adsorption, and re-desorption, and after re-activation by heating under vacuum. Filled and empty circles represent adsorption and desorption curves, respectively.

It should be noted that the discrepancy of the flexibility in ***flex*MOF(OH)** is attributed to the increased number of hydrogen bonds from ***as-flex*MOF(OH)** to ***cp-flex*MOF(OH)**, as revealed by the SCD analysis, owing to the single-crystal-to-single-crystal transformation (Fig. 5b and Fig. S20 in ESI†). In ***cp-flex*MOF(OH)**, the hydroxyl groups participate in hydrogen bonding with the carboxylate oxygens and the secondary amines from the macrocycles as well as the hydroxyl groups from other pendant arms to stabilize the ***cp*** structure by strong host-host interactions. Considering this aspect, while $CO_2$ molecules failed to open up the structure (Fig. S18, ESI†), certain guest molecules, which can make stronger host–guest interaction such as water, is expected to lead a structural flexibility, and water vapour sorption isotherm (Fig. 5c) shows that the introduction of polar water molecules can open the pores of ***cp-flex*MOF(OH)**; it adsorbs 144 cc $g^{-1}$ of water vapour at 298 K in two steps, at 0.08 and 0.65 relative humidity ($P/P_0$), and desorbs with a large hysteresis. The corresponding XRPD results, measured after water adsorption and re-activation by heating at 110 °C under vacuum, also verifies the significant and reversible structural transitions of ***flex*MOF(OH)** (Fig. S21, ESI†). Likely, ***flex*MOF(CN)** and ***flex*MOF($CH_2$)** also shows the stepwise adsorption profile for water vapour, which was similarly observed in the $CO_2$ sorption (Fig. S22, ESI†). Furthermore, methanol and benzene vapour isotherms of ***flex*MOF(OH)** were measured to prove the role of polar protic solvents in controlling

 

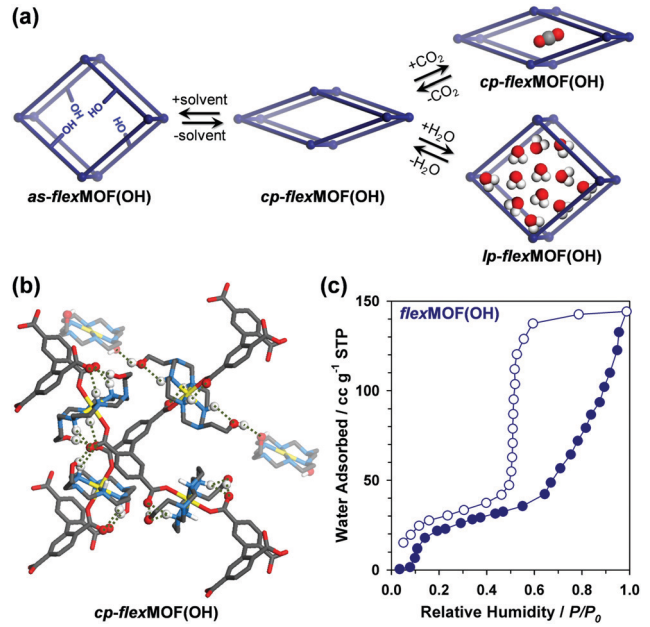


Fig. 5 (a) Schematic illustration of the phase transitions of ***flex*MOF(OH)** upon guest removal/reintroduction and adsorption/desorption of $CO_2$ and $H_2O$ molecules. (b) Hydrogen bonds of ***cp-flex*MOF(CN)** as represented by dotted lines, and (c) its water vapour isotherm at 298 K. Filled and empty circles represent adsorption and desorption curves, respectively.

the host–guest interaction and opening the closed pores. Resultingly, the pores of ***flex*MOF(OH)** was opened by methanol, but there was no adsorption by the non-polar benzene vapour (Fig. S25, ESI†).

In conclusion, we employed the Ni(II) macrocycle moiety with different pendant arms containing the nitrile, hydroxyl, or allyl groups, to demonstrate that such a MOF platform can readily grant and tune the flexibility based on the functional groups in the pores. Three isostructural MOFs exhibited distinct flexibility, including the gate-opening threshold pressure, sorption capacities, step steepness, and hysteresis. For ***flex*MOF(CN)** and **flexMOF($CH_2$)**, an intermediate new form was discovered from the $CO_2$-trapped ***np*** phase. Moreover, the hydroxyl group in ***flex*MOF(OH)** induced the strong host–host interaction *via* numerous hydrogen bonds in the ***cp*** phase, which could be attributed to the structural stabilisation, and ***flex*MOF(OH)** showed the responsive flexibility upon water over $CO_2$. Therefore, we envision that this pendant arm azamacrocycle-based MOF would not only provide insights for the rational design and fine-tuning of flexible MOFs but also enable their uses in a variety of practical applications.

This work was supported by the National Research Foundation of Korea (NRF) Grant funded by the Ministry of Science and ICT (No. NRF-2016R1A5A1009405, NRF-2017R1A2B4008757). X-ray crystallography analysis performed at 2D-SMC beamline (2018-3rd-2D-036) in PLS-II were supported by MSIT and POSTECH.

## Conflicts of interest

There are no conflicts to declare.

## Notes and references

1 (*a*) O. M. Yaghi, M. O'Keeffe, N. W. Ockwig, H. K. Chae, M. Eddaoudi and J. Kim, *Nature*, 2003, **423**, 705; (*b*) J.-R. Li, R. J. Kuppler and H.-C. Zhou, *Chem. Soc. Rev.*, 2009, **38**, 1477; (*c*) H. Sato, W. Kosaka, R. Matsuda, A. Hori, Y. Hijikata, R. V. Belosludov, S. Sakaki, M. Takata and S. Kitagawa, *Science*, 2014, **343**, 167.

2 (*a*) S. Horike, S. Shimomura and S. Kitagawa, *Nat. Chem.*, 2009, **1**, 695; (*b*) Z.-J. Lin, J. Lü, M. Hong and R. Cao, *Chem. Soc. Rev.*, 2014, **43**, 5867.

3 (*a*) J. H. Lee, S. Jeoung, Y. G. Chung and H. R. Moon, *Coord. Chem. Rev.*, 2019, **389**, 161; (*b*) A. Schneemann, V. Bon, I. Schwedler, I. Senkovska, S. Kaskel and R. A. Fischer, *Chem. Soc. Rev.*, 2014, **43**, 6062; (*c*) Z. Chang, D.-H. Yang, J. Xu, T.-L. Hu and X.-H. Bu, *Adv. Mater.*, 2015, **27**, 5432; (*d*) M. Shivanna, Q.-Y. Yang, A. Bajpai, S. Sen, N. Hosono, S. Kusaka, T. Pham, K. A. Forrest, B. Space, S. Kitagawa and M. J. Zaworotko, *Sci. Adv.*, 2018, **4**, eaaq1636; (*e*) P. Kanoo, R. Haldar, S. K. Reddy, A. Hazra, S. Bonakala, R. Matsuda, S. Kitagawa, S. Balasubramanian and T. K. Maji, *Chem. – Eur. J.*, 2016, **22**, 15864; (*f*) Y.-X. Shi, W.-X. Li, W.-H. Zhang and J.-P. Lang, *Inorg. Chem.*, 2018, **57**, 8627.

4 (*a*) C. Serre, C. Mellot-Draznieks, S. Surblé, N. Audebrand, Y. Filinchuk and G. Férey, *Science*, 2007, **315**, 1828; (*b*) G. Férey, *Z. Anorg. Allg. Chem.*, 2012, **638**, 1897.

5 (*a*) Y. Zhang, X. Zhang, J. Lyn, K.-I. Otaka, X. Wang, L. R. Redfern, C. D. Malliakas, Z. Li, T. Islamoglu, B. Wang and O. K. Farha, *J. Am. Chem. Soc.*, 2018, **140**, 11179; (*b*) A. W. Peters, K. Otake, A. E. Platero-Prats, Z. Li, M. R. DeStefano, K. W. Chapman, O. K. Farha and J. T. Hupp, *ACS Appl. Mater. Interfaces*, 2018, **10**, 15073; (*c*) H. Noh, C.-W. Kung, T. Islamoglu, A. W. Peters, Y. Liao, P. Li, S. J. Garibay, X. Zhang, M. R. DeStefano, J. T. Hupp and O. K. Farha, *Chem. Mater.*, 2018, **30**, 2193.

6 (*a*) Y. Sakata, S. Furukawa, M. Kondo, K. Hirai, N. Horike, Y. Takashima, H. Uehara, N. Louvain, M. Meilikhov, T. Tsuruoka, S. Isoda, W. Kosaka, O. Sakata and S. Kitagawa, *Science*, 2013, **339**, 193; (*b*) A. Schneemann, P. Vervoorts, I. Hante, M. Tu, S. Wannapaiboon, C. Sternemann, M. Paulus, D. C. F. Wieland, S. Henke and R. A. Fischer, *Chem. Mater.*, 2018, **30**, 1667; (*c*) C. M. McGuirk, T. Runčevski, J. Oktawiec, A. Turkiewicz, M. K. Taylor and J. R. Long, *J. Am. Chem. Soc.*, 2018, **140**, 15924; (*d*) P. Horcajada, F. Salles, S. Wuttke, T. Devic, D. Heurtaux, G. Maurin, A. Vimont, M. Daturi, O. David, E. Magnier, N. Stock, Y. Filinchuk, D. Popov, C. Riekel, G. Férey and C. Serre, *J. Am. Chem. Soc.*, 2011, **133**, 17839; (*e*) S. Henke, A. Schneemann, A. Wütscher and R. A. Fischer, *J. Am. Chem. Soc.*, 2012, **134**, 9464.

7 (*a*) S.-M. Hyun, T. K. Kim, Y. K. Kim, D. Moon and H. R. Moon, *Inorg. Chem. Commun.*, 2013, **33**, 52; (*b*) J. H. Lee and H. R. Moon, *J. Inclusion Phenom. Macrocyclic Chem.*, 2018, **92**, 237.

8 M. P. Suh, B. Y. Shim and T.-S. Yoon, *Inorg. Chem.*, 1994, **33**, 5509.

9 S.-M. Hyun, J. H. Lee, G. Y. Jung, Y. K. Kim, T. K. Kim, S. Jeoung, S. K. Kwak, D. Moon and H. R. Moon, *Inorg. Chem.*, 2016, **55**, 1920.

10 P. van der Sluis and A. L. Spek, *Acta Crystallogr., Sect. A: Found. Crystallogr.*, 1990, **46**, 194.

11 (*a*) A. Boutin, F.-X. Coudert, M.-A. Springuel-Huet, A. V. Neimark, G. Férey and A. H. Fuchs, *J. Phys. Chem. C*, 2010, **114**, 22237; (*b*) J.-R. Li, Y. Ma, M. C. McCarthy, J. Sculley, J. Yu, H.-K. Jeong, P. B. Balbuena and H.-C. Zhou, *Coord. Chem. Rev.*, 2011, **255**, 1791.

12 D. Dubbeldam, S. Calero, D. E. Ellis and R. Q. Snurr, *Mol. Simul.*, 2015, **41**, 1.

13 A.-X. Zhu, Q.-Y. Yang, A. Kumar, C. Crowley, S. Mukherjee, K.-J. Chen, S.-Q. Wang, D. O'Nolan, M. Shivanna and M. J. Zaworotko, *J. Am. Chem. Soc.*, 2018, **140**, 15572.